Growth-induced magnetic anisotropy and clustering in vapor-deposited Co-Pt alloy films

A. L. Shapiro, P. W. Rooney, M. Q. Tran, and F. Hellman
Department of Physics, University of California–San Diego, La Jolla, California 92093

K. M. Ring and K. L. Kavanagh
Department of Electrical and Computer Engineering, University of California–San Diego, La Jolla, California 92093

B. Rellinghaus and D. Weller
IBM Almaden Research Center, 650 Harry Road, San Jose, California 95120
(Received 28 April 1999; revised manuscript received 26 July 1999)

Polycrystalline and epitaxial (100)-, (110)-, and (111)-oriented $CoPt_3$ and $Co_{0.35}Pt_{0.65}$ films were deposited at various growth rates and over a range of growth temperatures from −50 to 800 °C. Films grown at moderate temperatures (200–400 °C) exhibit remarkable growth-induced properties: perpendicular magnetic anisotropy and large coercivity, as well as enhanced Curie temperature and low-temperature saturation magnetization. Magnetic measurements indicate significant Co clustering in these epitaxial fcc films. These properties are independent of crystallographic orientation, increase with increasing growth temperature, and vanish with annealing. We propose that the correlation between magnetic inhomogeneity, magnetic anisotropy, and enhanced moment is explained by clustering of Co into thin platelets in a Pt-rich lattice. This clustering occurs at the growth surface and is trapped into the growing film by low bulk atomic mobility.
[S0163-1829(99)09041-4]

INTRODUCTION

Vapor-deposited Co_xPt_{1-x} alloys of various compositions have been found to possess perpendicular magnetic anisotropy (PMA).[1–9] For certain compositions, oriented tetragonal or hexagonal long-range-ordered phases provide an obvious source of this anisotropy.[10] However, PMA also is present in fcc alloys, which should have cubic symmetry, where it appears to be a growth-induced effect, similar to amorphous Tb-Fe alloys.[11] The magnitude of this anisotropy can be quite large, significant fractions (~10%) of that found in the best Co/Pt multilayers, where the source of the anisotropy is clear.[12,13] The large PMA combined with large Kerr rotation at blue light frequencies exhibited by Co_xPt_{1-x} alloys makes this material a possible next-generation magneto-optic (MO) or perpendicular magnetic recording medium.[2]

At high temperature, in equilibrium, Co_xPt_{1-x} alloys have a face-centered cubic structure for all Co concentrations and are continuously soluble.[14] At lower temperatures, long-range chemical order develops, such that below 800 °C, near the $Co_{0.50}Pt_{0.50}$ composition, Co_xPt_{1-x} exhibits CuAu-type ($L1_0$) long-range order (LRO), and Cu_3Au-type ($L1_2$) LRO below 685 °C near the $Co_{0.25}Pt_{0.75}$ composition.[15] The $L1_0$ phase has tetragonal symmetry, and there have been observations of a hexagonal LRO phase at the $Co_{0.75}Pt_{0.25}$ composition,[16] but the $L1_2$ phase has cubic symmetry. Note that the $L1_2$ phase can be regarded as a chemically ordered fcc structure, specifically with Co atoms at the cube corners and Pt atoms at the face centers or, equivalently, with alternating (100) planes of pure Pt and CoPt. Our measurements have primarily been done on $Co_{0.25}Pt_{0.75}$ and $Co_{0.35}Pt_{0.65}$ samples. From the equilibrium phase diagram, for temperatures below the liquids, $Co_{0.25}Pt_{0.75}$ is structurally ordered (fcc), but chemically disordered above 685 °C and chemically ordered ($L1_2$) below 685 °C. The $Co_{0.35}Pt_{0.65}$ composition is similarly structurally ordered and chemically disordered (fcc) at high temperatures, but more complicated at lower temperatures, since it is near the two-phase $L1_0/L1_2$ region.

Perpendicular anisotropy previously reported in fcc Co_xPt_{1-x} thin films has been attributed to various mechanisms, ranging from remnants of oriented chemical LRO in $Co_{0.25}Pt_{0.75}$ samples,[4,5] to growth-induced heterogeneity for unspecified reasons,[3] to trapped-in surface phenomena such as surface segregation,[6,7] to compressive strain due to preferential pair coordination along the (111) growth direction,[7] to magnetically induced phase separation.[6] We have, however, shown[6] that samples exhibiting the strongest PMA have no LRO. Further evidence will be presented here for the existence of PMA in films with a variety of crystallographic orientations, with no LRO, suggesting that the anisotropy is not linked to the $L1_2$ or any other LRO phase, but is in fact a growth-induced effect, relatively independent of the underlying crystal structure. Recent work on sputtered samples has also found PMA in Co_xPt_{1-x} films with no LRO,[8] and even some of the early work supports this conclusion.[2] Through ongoing experiments with Ni-Pt alloys, which show somewhat similar effects, but have significantly lower Curie temperatures, we have also found that magnetic interactions cannot be the underlying cause.[17] Extended x-ray absorption fine structure (EXAFS) measurements on (111)-oriented $Co_{0.25}Pt_{0.75}$ films with PMA show increased Co-Co coordination in plane and increased Co-Pt coordination out of plane, within a fcc lattice, relative to films without PMA; this was suggested to be due to two-dimensional clustering of CO.[18,19] Angle-dependent magnetic circular dichroism experiments show both an increase and an asymmetry in the

magnitude of the Co orbital moment in and out of plane, again for (111) films, presumably reflecting the source of the magnetic anisotropy.[20]

As has been suggested in at least two papers,[6,7] an incomplete surface segregation which is trapped into the growing film seems a possible, although unproved, source of the anisotropic structure. In equilibrium, Co_xPt_{1-x} alloys are known to show nearly complete surface segregation.[21] Both the (111) and (100) surfaces are terminated with a pure Pt layer with significant Co enrichment of the second layer; this compositional modulation continues for approximately four atomic monolayers with an exponentially damped amplitude. The (110) surface has the reverse segregation, with the surface layer being Co rich and the second layer being Pt rich, and again an exponentially damped compositional modulation. The (100) surface undergoes a quasihexagonal reconstruction similar to that observed in pure (100) Pt.[21] The result of this reconstruction is that the surfaces of the (100) and (111) films should have the same symmetry during growth (both are triangular nets) with only a small difference in surface atom spacing, if the surface maintains an equilibrium structure during growth. This pattern of surface segregation has been observed for both fcc (chemically disordered) $Co_{0.2}Pt_{0.8}$ and $L1_2$ (LRO) $Co_{0.25}Pt_{0.75}$.[21] Note that the segregation means that the surface for all but the (100) orientation cannot be a bulk termination of the $L1_2$ phase, suggesting that surface energy dominates the long-range-order energy. Studies of Co monolayers deposited on a (111) Pt surface show that a stable, two-monolayer-thick, fcc (chemically disordered) alloy forms after annealing at 375 °C;[22] annealing at 630 °C results in diffusion of Co deeper into the Pt film. It would appear, then, that surface energetics suppress rather than favor the formation of the long-range-ordered phase in Co-Pt alloys.

In this paper, we report results of polycrystalline and (100)-, (110)-, and (111)-oriented single-crystalline Co_xPt_{1-x} ($x=0.25,0.35$) alloy films grown at different deposition rates and substrate temperatures. We have performed extensive vacuum annealing studies to explore the equilibrium states of these films. Structural characterization was done on a high-resolution x-ray diffractometer to study the crystal quality and chemical LRO. We characterized $M(T)$ and $M(H)$ at various temperatures, room-temperature torque, and magneto-optic Kerr effect (MOKE) to measure the Curie temperature, magnetization, anisotropy, and optical properties on samples with the same composition prepared under different conditions.

We find magnetic properties indicative of clustering of Co atoms in all samples with PMA. These properties include $M(T)$, which shows a broad magnetic ordering with a significantly enhanced magnetization onset (hundreds of °C), and $M(H)$ loops, which indicate inhomogeneity. We also find large enhancements in low-temperature saturation magnetic moments in the samples which exhibit PMA and enhanced magnetization onset, suggestive of large Co orbital contributions. We find that PMA in these Pt-rich Co_xPt_{1-x} samples is never present at the same time as $L1_2$ LRO; all samples with PMA are single-crystal fcc as measured by both x-ray scattering and transmission electron microscopy (TEM). We propose that Co clustering occurs on the growth surface and then is ''frozen'' in the bulk of those samples grown at temperatures for which bulk atomic mobility is low. It is possible that the source of this clustering is related to surface segregation. We suggest that the PMA originates at the Co/Pt interfaces of thin, flat Co platelets in a Pt matrix, similar to the anisotropy found in deliberately prepared Co/Pt multilayers; these platelets would explain not only the anisotropy, but the enhanced magnetic moment and broad magnetic onset with temperature. It is interesting to note that the anisotropy in these seemingly cubic materials, prepared by codeposition, approaches 10% of that found in the best Co/Pt multilayers.[12,13]

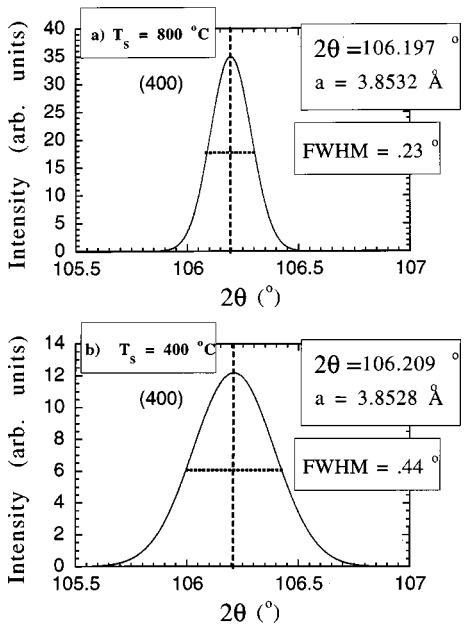

FIG. 1. High-resolution θ-2θ scans about the (400) x-ray reflection from (100)-oriented $Co_{0.25}Pt_{0.75}$ films grown at (a) 800 °C and (b) 400 °C.

SAMPLE PREPARATION AND STRUCTURAL CHARACTERIZATION

Epitaxial (100), (110), and (111) Co_xPt_{1-x} films were grown on (100) MgO and NaCl, (110) MgO, and (0001) Al_2O_3, respectively, and polycrystalline Co_xPt_{1-x} films on amorphous-SiN-coated Si substrates. Samples were grown at deposition temperatures from -50 to 800 °C with $x=0.25\pm0.02$ or 0.35 ± 0.02 as determined by electron microprobe and Rutherford backscattering.[23] The error represents the variation in composition of different samples rather than the uncertainty in the measurement. The films were deposited from individual Co and Pt sources using electron beam coevaporation. The total deposition rate was varied between 0.012 and 1.5 Å/s. The base pressure of our vacuum system is 9.5×10^{-11} Torr and the pressure during deposition was 3.0×10^{-10} Torr. The film thickness was varied from 300 to 3000 Å and was measured using low-angle x-ray interference fringes. No significant dependence on film thickness was found in any of the magnetic properties.

Figure 1 shows high-resolution, high-angle θ-2θ scans about the (400) x-ray reflections from (100)-oriented $Co_{0.25}Pt_{0.75}$ films grown at 800 and 400 °C. The data were acquired using a four-crystal [(220) Ge] monochrometer on

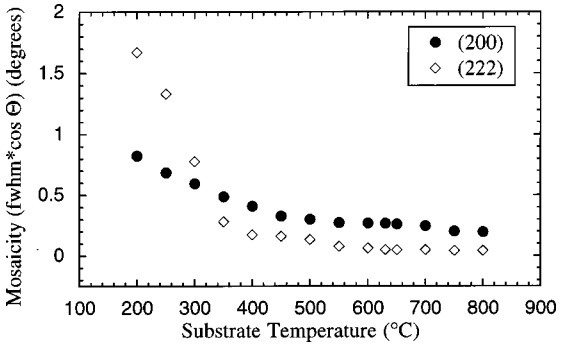

FIG. 2. Mosaic spread (determined by triple-axis x-ray measurements) in as-deposited (111) and (100) $Co_{0.25}Pt_{0.75}$ films as a function of substrate temperature during growth. Rocking curves were measured about the (200) and (222) reflections of the (100)- and (111)-oriented films, respectively. Mosaicity increases with decreasing growth temperature except for (111)-oriented film grown at −50 °C (not shown in figure) which was grown on a Pt seed layer and had a mosaic spread of 1.45°. Error bars are smaller than symbol size and are not displayed.

the incident beam side (Cu $K\alpha$ radiation) and a single (220) Ge monochrometer on the exit beam side. The film grown at 800 °C is chemically disordered ($S<0.1$, where S is the long-range-order parameter), indicating that we were able to quench the sample from 800 °C to room temperature without developing LRO. LRO was also below the detectable limits ($S<0.1$) in the film grown at 400 °C, as it was in all films deposited at temperatures below 550 °C. The lattice constants of the films deposited at 400 and 800 °C are identical to within 0.03%, and there is no evidence of any kind of distortion or second peak in the reflection from the film grown at 400 °C. The greater width of the reflection from the 400 °C film is a manifestation of a larger number of structural defects in this film relative to the film grown at 800 °C, as will be further discussed below. These defects and low-angle grain boundaries limit the coherence size of fcc domains seen by x-ray reflections (e.g., from the width seen in Fig. 1) to less than 500 Å.

High-resolution x-ray diffraction measurements of the (400), (333), and (330) reflections from each film, both (100) and (111) orientations, show that strain is less than 0.03% in all cases, consistent with previous measurements.[4] There is therefore no significant structural difference in the lattice between the in-plane and perpendicular directions on the length scale measured by x-ray diffraction.

Figure 2 shows the full width at half maximum (FWHM) of the rocking curve about the (200) and (222) reflections of the (100)- and (111)-oriented samples, respectively, as a function of substrate temperature during growth. In general, the mosaic spread is a strong function of the growth temperature and we see that down to 200 °C the width of the rocking curve increases as the growth temperature is reduced. These rocking curves are also consistent with fcc coherent domain sizes of under 500 Å, limited by structural defects which are seen in TEM. The film grown at −50 °C (Ref. 23) (not shown in the figure) has a narrower rocking curve than films grown at 200 °C. This is, possibly, a manifestation of reentrant layer-by-layer growth known to occur in vapor-deposited Pt films or more likely due to the use in this film of a Pt seed layer deposited immediately before deposition of the alloy.

As noted earlier, $Co_{0.25}Pt_{0.75}$ has a Cu_3Au-type ($L1_2$) long-range-ordered phase in which Co atoms occupy the corner sites of a fcc unit cell and Pt atoms occupy the face sites. In our previous work we showed the dependence of the magnitude of the long-range-order parameter S on growth temperature, for the as-deposited $Co_{0.25}Pt_{0.75}$ films.[6] S is zero for films grown above 675 °C, as expected from the equilibrium bulk phase diagram. Below 675 °C, S matches the increasing order with decreasing temperature seen in the bulk equilibrium curve down to 630 °C. Below 630 °C the as-grown LRO falls significantly below the bulk equilibrium value. Estimates of the domain size of the LRO phase based on the width of the x-ray superlattice peaks show that domains are small (of the order of 150 Å in the film with maximum LRO).

Reflection high-energy electron diffraction (RHEED) patterns observed during growth of the epitaxial films showed vertical diffraction lines with no sign of rings and low diffuse scattering, indicating good crystal quality for all films even at 3000 Å thickness. Pt seed layers are needed to get epitaxial growth below 200 °C. At high temperature, 600 °C, where we find the films as-grown possess significant $L1_2$ LRO, an unreported five-fold surface reconstruction was observed in RHEED. Morphological changes take place in the as-deposited film in the first one to five monolayers of the as-deposited film. The first two monolayers of the film show a spotted RHEED reflection, consistent with extremely flat layers, while subsequent layers yield an image with long, uniform streaks. Atomic force microscopy images of the top surfaces of 3000-Å-thick films show significant roughness and islanding.

EXAFS measurements have been made. Full analyses are not yet completed and will be reported in a future publication.[24] The EXAFS measured on the Co absorption edge shows significant enhancement in in-plane Co-Co coordination numbers for films grown at 400 °C, consistent with results by other workers.[18,19] Out-of-plane coordination was not measured.

Transmission electron microscopy (TEM) was used to examine the structure of 600-Å-thick (100) $Co_{0.25}Pt_{0.75}$ samples deposited on both MgO and NaCl. The NaCl substrates were dissolved in water. The samples deposited on MgO were etched in water at 80 °C for a period of approximately 1 week, after which time the sample lifts off the substrate. The disadvantage of this technique is that only very small sample flakes are recovered. Figures 3(a) and 3(b) show bright-field TEM micrographs of (100)-oriented $Co_{0.25}Pt_{0.75}$ films deposited on (100) MgO at 400 °C and (100) NaCl at 300 °C, respectively. In both cases, the sample is single crystalline as seen from the selected area diffraction patterns (SAD), shown in the insets. The SAD patterns show that the structure is fcc with a lattice spacing of 3.83 ± 0.03 Å, consistent with x-ray measurements. LRO peaks [e.g., (100)] were carefully looked for and not seen. The contrast seen in Fig. 3(a) is from dislocations, likely originating from thermal and lattice mismatch relaxation processes. The tiling seen in Fig. 3(b) is probably the result of growth domains influenced by the surface structure of the NaCl substrate, etched away during (TEM) sample preparation.

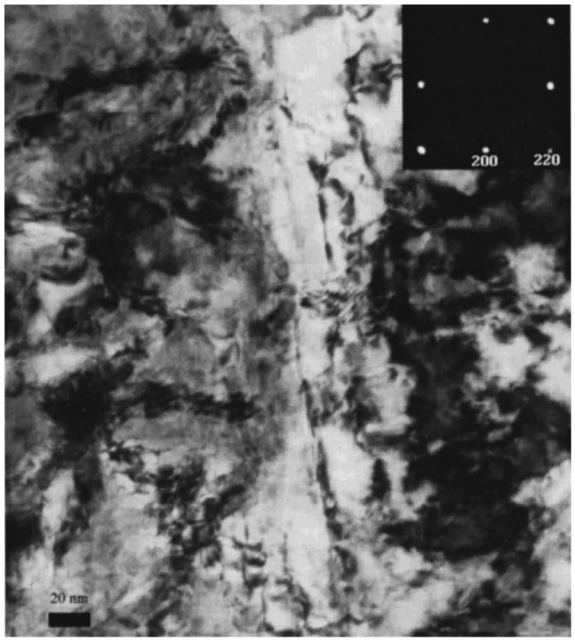

(a)

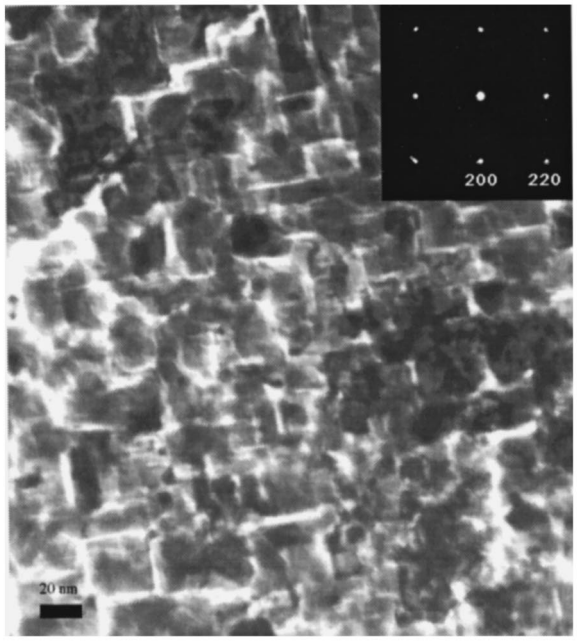

(b)

FIG. 3. Bright-field, plan-view TEM micrographs of 600-Å-thick $Co_{0.25}Pt_{0.75}$ films deposited at (a) 400 °C on MgO (100) and (b) 300 °C on NaCl (100). The selected-area diffraction patterns shown in the insets are from a (100) pole. The contrast in (a) is consistent with dislocations. The contrast in (b) comes from a semi-regular rectangular tiling aligned with the (100) in-plane directions and is probably due to growth domains nucleated on the NaCl substrate.

MAGNETIC MEASUREMENTS

We have studied the magnetic transition $M(T)$ in $Co_{0.25}Pt_{0.75}$ and $Co_{0.35}Pt_{0.65}$ samples as a function of growth temperature, using a vibrating sample magnetometer (VSM). A Pt-Rh thermocouple was mounted directly on the quartz VSM sample rod, and the rod was immersed in temperature-controlled flowing Ar gas. Each sample was first technically saturated along the easy axis or plane of magnetization: then, the external field was reduced to 200 Oe and the magnetization was measured upon heating.

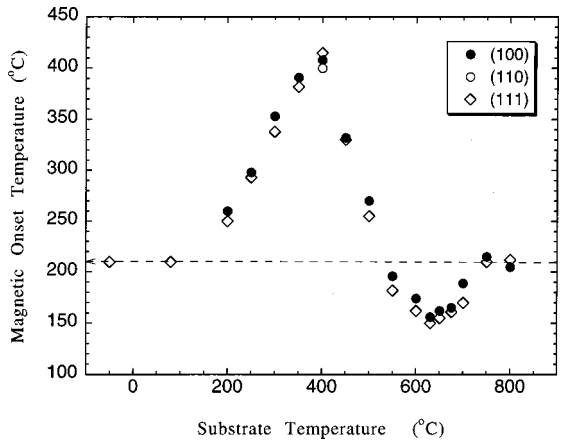

FIG. 4. Magnetic onset temperature of (100), (110), and (111) as-deposited $Co_{0.25}Pt_{0.75}$ films as a function of substrate temperature during growth where onset temperature is defined to be the temperature at which the magnetization rises to 5% of its value at 25 °C. The dashed line shows T_c for the fcc phase; T_c for the fully ordered $L1_2$ phase is 0 °C. Films grown at 80 °C and −50 °C were grown on a thin (25–50 Å) Pt seed layer (without which they were not epitaxial). Error bars are smaller than symbol size and are not displayed.

In previous work[6] we showed that (100) and (111) films of $Co_{0.25}Pt_{0.75}$ deposited at 700–800 °C show a sharp magnetic transition at an ordering temperature of 210 °C, as expected for the chemically disordered fcc phase. This result shows that the as-deposited film was successfully quenched from a 700–800 °C growth temperature to room temperature and may be thermally cycled up to (at least) 210 °C without significant annealing; annealing experiments described below show that thermal cycling up to 400 °C (for brief times) causes no changes in any of the films described here. Films grown at growth temperatures between 500 and 650 °C show a slightly broadened magnetic transition and a lowered onset temperature due to partial LRO.[6,25,26] Films grown between 200 and 450 °C have a broad magnetic transition and an increased onset temperature (by 50–200 °C). Films grown at low temperature (−50 and 80 °C) show once again a sharp magnetic transition at the fcc Curie temperature of 210 °C. Figure 4 is a plot of the magnetic onset temperature as a function of deposition temperature in as-deposited $Co_{0.25}Pt_{0.75}$ films for all three orientations. The dependence on growth temperature is the same as was found previously[6] and does not depend on orientation of the film. It also does not depend on the film thickness (from 300 to 3000 Å at least).

The saturation magnetization M_S measured far below T_C follows the same trend as the onset temperature in as-deposited $Co_{0.25}Pt_{0.75}$ samples. Figure 5 shows M_S at 5 K of $Co_{0.25}Pt_{0.75}$ samples deposited at different temperatures. The magnetic moment per stoichiometric unit cell (for every one Co and three Pt atoms) varies from $\mu=(1.85\pm0.1)\mu_B$ in the $T_S=630$ °C sample (partial LRO) to $(2.1\pm0.1)\mu_B$ in the $T_S=800$ °C sample (fcc phase) to $(2.7\pm0.1)\mu_B$ in the $T_S=400$ °C sample. The uncertainty in these values is domi-

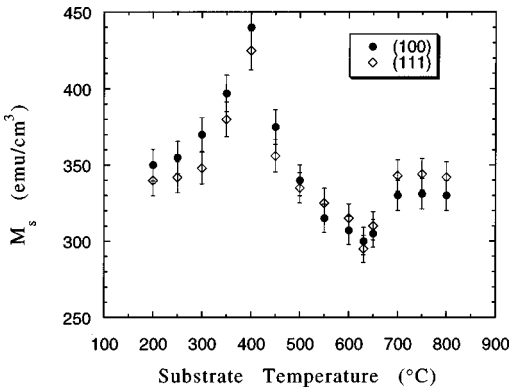

FIG. 5. Low-temperature saturation magnetization M_S of as-deposited $Co_{0.25}Pt_{0.75}$ films as a function of substrate temperature during growth. M_S was determined from $M(H)$ curves measured at 5 K with H along the easy axis, with a vibrating sample magnetometer.

nated by uncertainty in the sample volume. In all cases the moment is higher than can be accounted for by the moment typically quoted for the Co $[(1.74-1.78)\mu_B/\text{atom}]$; the additional moment for both the fcc and $L1_2$ phases is traditionally associated with magnetization of the Pt and is larger in the fcc phase ($\mu_{Pt}=0.24\mu_B$) than in the $L1_2$ phase ($0.1\mu_B$).[27,28] Note, however, that $2.7\mu_B$ for $T_S=400\,°C$ is considerably higher than is reported for either the fcc or $L1_2$ phase, even including the Pt enhancements found there; since M_S is an average property, the excess is not easily explained. In Co/Pt multilayers, enhancements in the Co orbital moment at the interfaces of $0.07\mu_B$ have been measured.[29] If we take the maximum of all these values, $(1.78+0.07)\mu_B$ for Co and $0.24\mu_B$ for each Pt$=2.6\mu_B$ per unit cell, we nearly reach the observed value of $2.7\mu_B$, but this implies that all Co is at planar interfaces with Pt, as in a thin multilayer, and all Pt has three Co neighbors, as in fcc $CoPt_3$. Angular-dependent magnetic circular dichroism measurements of (111) $CoPt_3$ grown at 417 °C have suggested a Co orbital moment enhancement of $0.16\mu_B$,[20] consistent with our magnetization measurements. We note also the strong correlation of the magnetic onset temperature with increased low-temperature magnetic moments, both in this work and for the literature fcc and $L1_2$ phases.

Figures 6(a)–6(d) are plots of the parallel and perpendicular hysteresis loops measured at room temperature of $Co_{0.25}Pt_{0.75}$ samples deposited at, respectively, 800, 630, 400, and −50 °C. The samples deposited at 800, 630, and −50 °C all have an easy plane, with an anisotropy field (from hard-axis measurements) $H_K \leqslant 4\pi M_S$ corresponding to shape anisotropy plus (for 630 and −50 °C) a small intrinsic perpendicular anisotropy. Samples grown near room temperature (80 °C) have $M(H)$ curves identical to that shown for 800 °C, with $H_K=4\pi M_S$. The 400 °C samples shows a perpendicular easy axis, significant coercivity, and remanence in the hysteresis loop. Thin samples (300 Å) grown at 400 °C have similar $M(H)$ curves, with similar coercivity, but the hysteresis loop is more square, giving much higher zero-field magnetic remanence than that seen in Fig. 6(c). Polycrystalline samples grown at 400 °C have much larger coercivity (over 10 000 Oe at room temperature) and full remanence ($M_r=M_S$). Films grown at temperatures between 200 and 400 °C show $M(H)$ curves similar to those of the 400 °C sample. Large coercivity and remanence, attributable to inhomogeneity in the sample, are only found in samples with

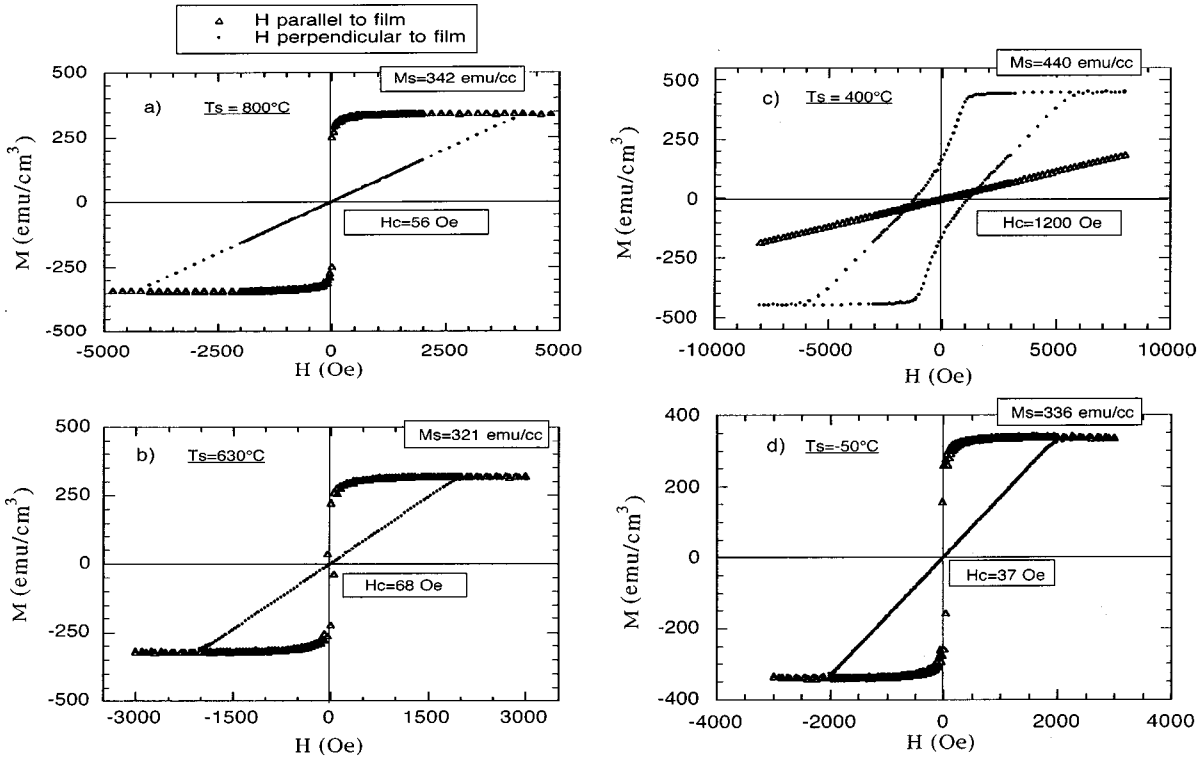

FIG. 6. $M(H)$ curves, with H parallel and perpendicular to the film plane, acquired at room temperature for (111) $Co_{0.25}Pt_{0.75}$ 3000-Å-thick films grown at (a) 800 °C, (b) 630 °C, (c) 400 °C, and (d) −50 °C.

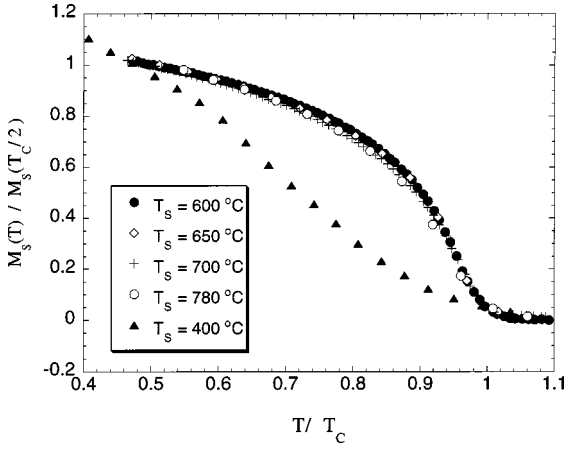

FIG. 7. Normalized magnetization as a function of temperature normalized by T_c for each film, measured upon heating in a 200 Oe external field for as-deposited (111) $Co_{0.35}Pt_{0.65}$ films grown at 780, 700, 650, 600, and 400 °C. M was measured with H applied along the easy axis or plane of magnetization (in plane for 780, 700, 650, and 600 °C, perpendicular for 400 °C). The films grown at 600 °C or above all have a sharp, ferromagnetic onset near a well-defined Curie temperature. The film grown at 400 °C exhibits a very broad transition. Films grown at other temperatures show intermediate behavior.

significant PMA and enhanced magnetic onset temperature. Samples grown at both higher and lower temperatures show low coercivity, implying a more homogeneous sample.

Similar results are found for $Co_{0.35}Pt_{0.65}$. Figure 7 shows the normalized magnetic moment as a function of reduced measurement temperature for (111)-oriented $Co_{0.35}Pt_{0.65}$ films deposited at 780, 700, 650, 600, and 400 °C. As in the $Co_{0.25}Pt_{0.75}$ samples, the shape of the magnetic transition is sharp and nearly identical for the films deposited at the higher temperatures, but it is notably broader for the film deposited at 400 °C. Figure 8 is a plot of the magnetic onset temperature of $Co_{0.35}Pt_{0.65}$ films as a function of deposition temperature. The onset temperature is enhanced by almost 200 °C in the $Co_{0.35}Pt_{0.65}$ film deposited at 400 °C film compared to the one deposited at 800 °C. In $Co_{0.35}Pt_{0.65}$, unlike $CoPt_3$, small LRO peaks (e.g., 100) were observed in nearly all films. This may be a consequence of the proximity of these 35 at. % samples to the two-phase boundary. The integrated intensity of these peaks is very small (the LRO parameter S is less than 0.1).

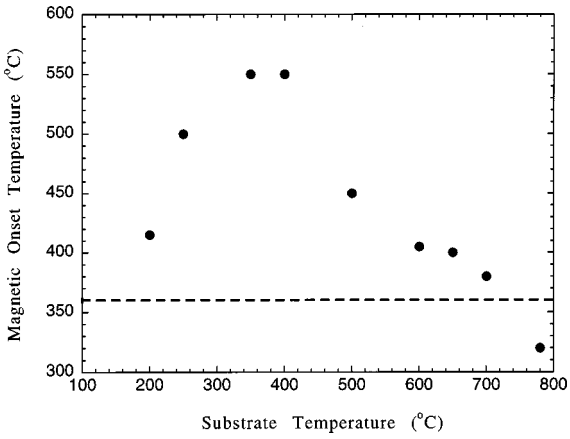

FIG. 8. Magnetic onset temperature of as-deposited (111)-oriented $Co_{0.35}Pt_{0.65}$ films as a function of substrate temperature during growth where onset temperature is defined to be the temperature at which the magnetization rises to 5% of its value at 25 °C. The dashed line shows T_c for the fcc phase. Error bars are smaller than symbol size and are not displayed.

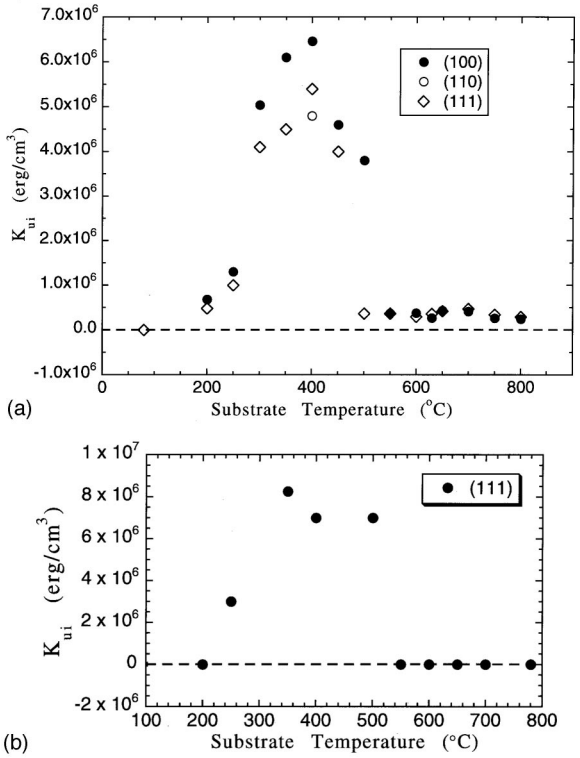

FIG. 9. Intrinsic, uniaxial, perpendicular anisotropy in as-deposited (a) (100), (110), and (111) $Co_{0.25}Pt_{0.75}$ and (b) (111) $Co_{0.35}Pt_{0.65}$ films as a function of substrate temperature during growth (shape anisotropy contribution removed).

We measured the perpendicular magnetic anisotropy at room temperature in Co_xPt_{1-x} alloy films through torque magnetometry. The net anisotropy K' was determined using Miyajima's 45° method,[30] and the intrinsic anisotropy K_{ui} is given by $K_{ui}=K'+2\pi M_S^2$. For some samples, with large M, K_{ui} was determined from the $M(H)$ curves using the expression $K'=(H_K^* M_S)/2$, where H_K is the field value at which the magnetization along the hard axis first reaches its saturation value. Torque magnetometry measurements show a large intrinsic perpendicular uniaxial magnetic anisotropy in samples deposited at temperatures from 200 to 450 °C with a maximum at 400 °C, for $Co_{0.25}Pt_{0.75}$. Figure 9(a) shows the intrinsic anisotropy K_{ui} as a function of deposition temperature in $Co_{0.25}Pt_{0.75}$ samples for the three orientations, as measured by torque magnetometry. The shape anisotropy is less than 15% of the peak perpendicular anisotropy. Figure 9(b) shows similar data for $Co_{0.35}Pt_{0.65}$, determined from $M(H)$ curves.

The magnetic ordering onset temperature $M(T)$ curve and anisotropy for (100) $Co_{0.25}Pt_{0.75}$ samples grown epitaxially on NaCl were the same as for samples deposited on (100) MgO, but the coercivity was substantially higher. The higher coercivity is probably due to a higher number of defects at a spacing relevant to domain wall nucleation and pinning

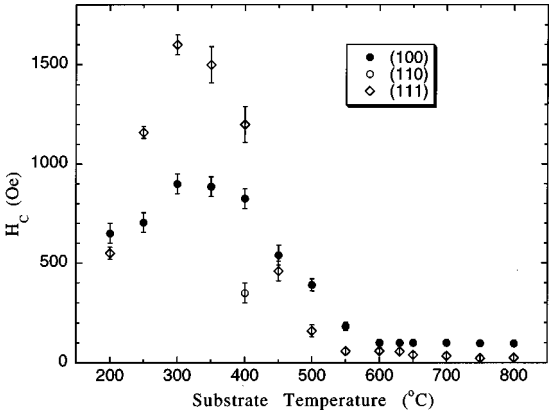

FIG. 10. Room-temperature coercivity of as-deposited epitaxial $Co_{0.25}Pt_{0.75}$ films as a function of substrate temperature during growth. The coercivity in polycrystalline films is approximately 10× larger than that shown here.

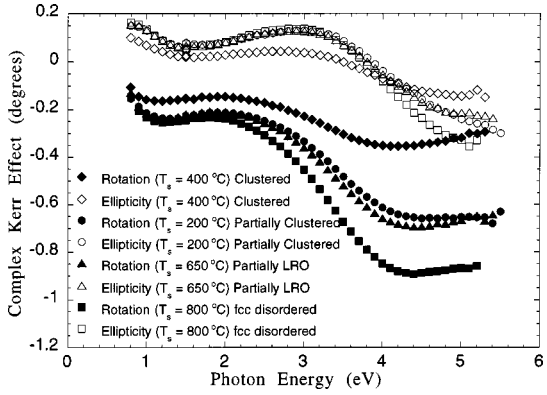

FIG. 11. Ellipticity and Kerr rotation for as-deposited $Co_{0.25}Pt_{0.75}$ films [(100) epitaxial]. The samples deposited at 400 and at 200 °C have perpendicular anisotropy. The 800 and 650 °C samples have in-plane (shape) anisotropy. All samples were measured by polar Kerr using perpendicular saturating magnetic fields (±20 kOe); see Ref. 31 for details.

(hundreds of Å; see Fig. 3) in the sample deposited on NaCl, which has a rougher surface than polished MgO.

There is complete correlation between T_C and M_S enhancements and anisotropy in our Co_xPt_{1-x} samples. The rise, peak, and rapid dropoff of the anisotropy and of the Curie temperature and low-temperature moment enhancement occur at the same deposition temperatures, independent of crystallographic orientation of the film. Films with perpendicular anisotropy also show significant coercivity, shown in Fig. 6(c) and plotted as a function of growth temperature in Fig. 10. Unlike anisotropy, however, coercivity depends strongly on orientation and peaks not at 400 °C, but closer to 300 °C, consistent with results of previous workers on evaporated and sputtered samples. These variations will be discussed further below, but are presumably a result of microstructural differences (see, e.g., mosaicity shown in Fig. 2) which have a strong effect on coercivity.

Complex polar MOKE spectra (polar Kerr angle and ellipticity) were measured in air and at room temperature, covering photon energies between 0.8 and 5.3 eV. Fields of +/−20 kOe, sufficient to saturate the magnetization in the film normal direction, were applied during the measurements (see Ref. 31 for more details). Figure 11 shows the rotation and ellipticity of the reflected light in the MOKE measurement as a function of energy. We note that all samples have an enhanced rotation at blue light energies (~4 eV). The homogeneous alloy (T_S=800 °C) has the largest Kerr rotation (a rotation of 0.8°, which is significantly larger than previously measured in either $Co_{0.25}Pt_{0.75}$ or in Co/Pt multilayers[2]), but has no PMA. The sample with maximum PMA (grown at 400 °C) has considerably smaller Kerr rotation. We note the technologically important result that the sample deposited at 200 °C has significant PMA *and* a Kerr rotation higher than that found in multilayers, combining two important storage medium properties at a relatively low deposition temperature.

We have vacuum annealed films grown at various deposition temperatures at temperatures ranging from 200 to 800 °C for times ranging from 1.5 to 500 h. We have found that annealing at temperatures above 400 °C drives the samples toward the accepted bulk equilibrium, either the chemically LRO state or the chemically disordered fcc state, depending on the annealing temperature. Specifically, annealing any sample for 100 h at 800 °C results in a film with no PMA and a Curie temperature of 210 °C, the same as that found in films deposited at 800 °C. Annealing at temperatures between 450 and 685 °C, the LRO temperature, results in gradual formation of the LRO phase, with a consequent gradual drop in Curie temperature and elimination of PMA.

Annealing at temperatures less than 400 °C left the anisotropy, T_c, and the shape of the $M(T)$ curve unchanged in all samples. 400 °C is close to one-third of the melting temperature of $CoPt_3$ and, hence, an approximate temperature at which appreciable bulk mobility is expected. At 400 °C, we find strong effects of the length of annealing time. Annealing a sample grown at 400 °C for 100 h at 400 °C results in a 20% drop in PMA and no noticeable change in the onset temperature. A 500 h anneal at 400 °C results in the PMA relaxing away, a drop in the magnetic onset temperature, and a sharpening of the magnetic transition. Figure 12 shows the effect of annealing a sample deposited at 400 °C at temperatures of 400 °C and above. At higher annealing temperatures

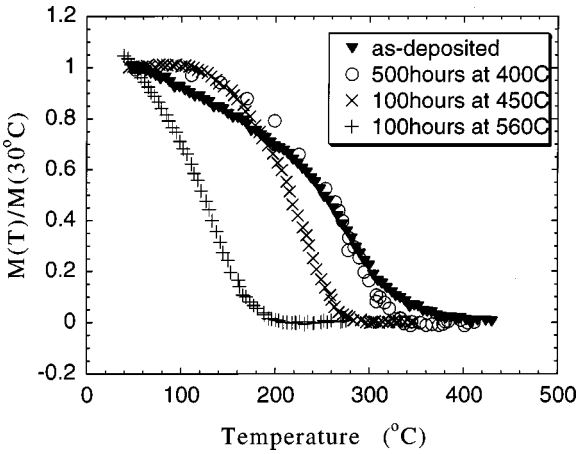

FIG. 12. Normalized $M(T)$ of $Co_{0.25}Pt_{0.75}$ samples deposited at T_s=400 °C and vacuum annealed at temperatures and times shown in the legend. $M(T)$ was measured in H of 200 Oe applied along the easy axis or plane as measured at room temperature, after magnetically saturating in 10 000 Oe.

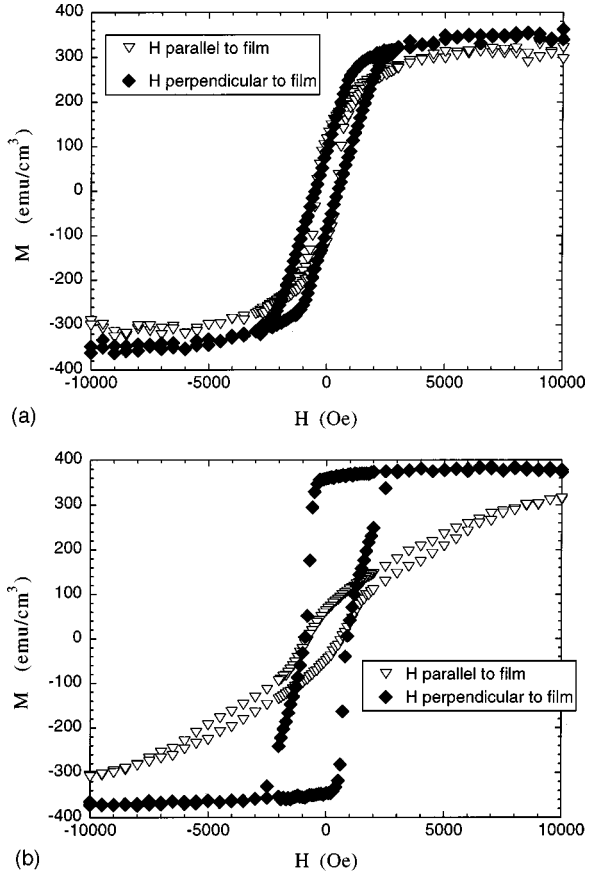

FIG. 13. $M(H)$ curves, with H parallel and perpendicular to the film plane, acquired at room temperature for 300 Å (111) $Co_{0.25}Pt_{0.75}$ films grown at 250 °C at a rate of (a) 1.5 Å/s and (b) 0.012 Å/s. In (a), there is no preference for the moment to lie in or out of plane, meaning that a small intrinsic PMA is balanced by shape anisotropy. In (b), the easy axis is perpendicular with a large intrinsic anisotropy energy.

the anisotropy relaxes away completely and the magnetic onset temperature drops below that of the homogeneous alloy, due to the formation of the LRO phase.

We have also annealed samples deposited at 200, 600, and 800 °C at 450 °C for 100 h. The sample deposited at 200 °C loses its PMA, and the magnetic ordering onset drops to 140 °C, while the magnetic transition sharpens. The sample deposited at 600 °C, which was partially long-range ordered in the as-deposited state, undergoes the smallest change in Curie temperature. Finally, the sample deposited at 800 °C undergoes a 20 °C drop in Curie temperature and the magnetic transition slightly broadens, due presumably to development of partial LRO.

We have investigated the effect of deposition rate on the anisotropy and clustering in $Co_{0.25}Pt_{0.75}$ samples deposited at 400 and 250 °C. At 400 °C varying the deposition rate by an order of magnitude has no effect on PMA or on the magnetic onset temperature enhancement: samples deposited at 0.15 and at 1.3 Å/s have the same $M(T)$ profile and identical $M(H)$ hysteresis loops at room temperature. For substrate temperatures of 250 °C, however, increasing the deposition rate produces a marked decrease in PMA. Figure 13(a) is a hysteresis loop of a $Co_{0.25}Pt_{0.75}$ sample deposited at a rate of 1.5 Å/s. The perpendicular and parallel hysteresis loops are

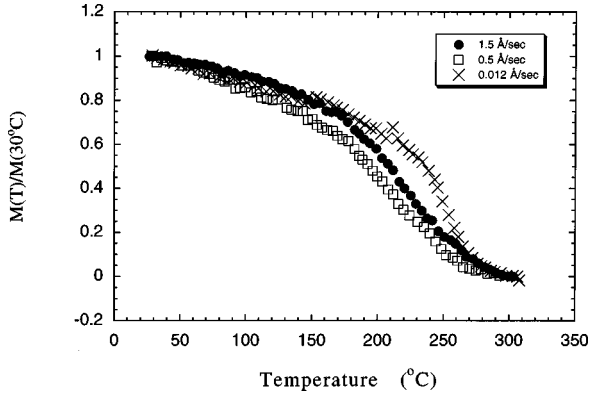

FIG. 14. Normalized $M(T)$ measured upon heating in a 200 Oe perpendicular applied field, after magnetically saturating at room temperature, for as-deposited 300-Å-thick (111) $Co_{0.25}Pt_{0.75}$ films grown at 250 °C at three different deposition rates.

nearly the same, implying that the intrinsic anisotropy energy is on the order of the shape anisotropy, $K_{ui} \sim 6 \times 10^5$ erg/cm^3. When $Co_{0.25}Pt_{0.75}$ is deposited at a rate 100 times slower, 0.012 Å/s [Fig. 13(b)], the sample exhibits PMA with a much larger anisotropy energy ($K_{ui} \sim 2.6 \times 10^6$ erg/cm^3). Figure 14 shows $M(T)$ data for $Co_{0.25}Pt_{0.75}$ deposited at 250 °C at three different deposition rates. There is little difference between these three curves: the sample deposited at the slowest rate (0.012 Å/s) has a somewhat sharper transition than the samples deposited at higher rates, but the magnetic onset temperature is the same in all of the samples.

We have deposited a series of Co-Ag samples at a variety of compositions and growth temperatures between 200 and 400 °C to probe Co clustering in an alloy with a positive energy of mixing. Various magnetic behaviors were seen, but no samples showed the broad $M(T)$ curves seen in Co-Pt alloys.

DISCUSSION

Analyses of the magnetic and structural data lead to the conclusion that the Co atoms are clustering in as-deposited samples grown near 400 °C despite the fact that they remain structurally single crystal. The broadened magnetic transition seen in samples deposited near 400 °C is indicative of inhomogeneity in the sample, while the enhanced magnetic onset (200 °C higher than either the fcc or $L1_2$ phases of the same composition) indicates clustering of the Co atoms within the alloy matrix. An increased number of Co-Co nearest neighbors leads to a stronger exchange coupling and a higher ordering temperature. A distribution of cluster sizes results in a distribution of magnetic transition temperatures and hence a slowly rising moment with decreasing temperature. Co clustering could also account for the large coercivity seen in these samples and not seen, for example, in the sample grown at −50 °C. The overall shape of the hysteresis loops is explained by well-developed models of stripe domains in materials with PMA,[32–34] but the significant remanence and coercivity are the result of irreversible magnetization processes and an indication of inhomogeneity of some type.[33]

Uniaxial magnetic anisotropy is found in samples that are structurally cubic as seen in x-ray measurements, for all three

orientations [(100), (110), and (111) and polycrystalline]. It is difficult to construct a mechanism of residual LRO which explains PMA in (111)- and (110)-oriented $Co_{0.25}Pt_{0.75}$ films since the compositional ordering which is the $L1_2$ phase occurs along the (100) directions. Furthermore, neither TEM nor x-ray diffraction measurements show LRO in films with PMA (e.g., grown at 400 °C). Measurements of the mosaic spread (Fig. 2) show no correlation between crystal quality and perpendicular anisotropy. Crystal quality does not begin to appreciably degrade until the deposition temperature reaches 250 °C for (111)-oriented samples and never shows a sharp change in (100)-oriented samples, while PMA peaks at 400 °C and is found in samples deposited at temperatures up to 450 °C.

We suggest that uniaxial anisotropy in this apparently cubic system (as measured by x rays) is due to the Co clustering discussed above, specifically in the form of Co platelets within a Pt-rich matrix, parallel to the surface. This atomic arrangement results in a structure locally similar to a multilayer, but incoherent across the sample, so that x-ray measurements see only the long-range fcc order. Previous work on Co/Pt multilayers[2,12,13] has demonstrated that clean Co/Pt interfaces are a source of large PMA and that thin layers of Co are required for the moment to be perpendicular. Previous work on ultrathin Co layers grown on Cu (Ref. 35) has shown that the Curie temperature of ultrathin fcc Co is on the order of 200–400 °C between two and three monolayers, similar to what is seen here, supporting the suggestion that the platelets must be thin, pure Co in a Pt matrix.

The strong correlation of enhanced low-temperature magnetic moments with magnetic onset temperature and with perpendicular anisotropy further supports the model of thin Co platelets. To obtain such large values of moment (up to $2.7\mu_B$ for $T_s = 400$ °C) requires both significant Pt polarization and Co orbital moment. This large orbital moment also gives rise to the perpendicular anisotropy, similar to what is found in Co/Pt multilayers, due to Co at the planar Pt interfaces.

Magneto-optic Kerr effect measurements (Fig. 11) show a strong similarity between the MO spectrum of our most clustered sample (grown at 400 °C) and previously measured multilayers.[2] The MOKE spectrum, particularly near 4 eV, is quite sensitive to the Pt environment due to Pt polarization effects. In multilayers, polarization occurs at the interfaces. In alloys, more Co nearest neighbors cause increased Pt polarization and hence an increased contribution to the MOKE signal. The enhanced Kerr effect at 4 eV photon energies in Fig. 11 for the film grown at 800 °C suggests a more alloy-type behavior whereas the reduction in our most clustered films points to a two-dimensional-like environment. The magnitude of the 4 eV MOKE signal thus is not simply proportional to the net moment of the sample, which is significantly larger in the clustered films (see Fig. 5).

We point out that the *magnitude* of the PMA, not just its presence or absence, correlates closely with the value of the initial magnetic onset temperature in as-deposited samples. The size of the clustered platelets could be determinative of the onset temperature, while the smoothness of the Co/Pt interfaces determines the strength of the PMA. It is reasonable to postulate that greater Co clustering leads to larger, more defined platelets. This would explain why the onset temperature and the anisotropy increase monotonically with deposition temperature up to 400 °C. Annealing and deposition rate may have slightly different effects on the size of the platelets than they do on the smoothness of the interfaces, explaining why, for example, annealing and faster deposition rates reduce anisotropy more quickly than T_c onset.

As previously mentioned, the peak in the coercive force occurs at a deposition temperature of 300 °C, well below the peak in anisotropy. The coercivity convolves the value of the anisotropy and crystal quality, explaining why coercivity depends more strongly than anisotropy on the film orientation. A sample with more internal dislocations is likely to increase pinning of domain walls. The monotonically increasing mosaic spread with decreasing T_S explains why greater coercivity is found in some samples with less anisotropy.

The appearance of Co platelets in a material with a negative energy of mixing (favoring ordering, not phase separation) is unexpected. We suggest that the Co platelets are a growth-surface-driven effect which disappears with annealing as the sample relaxes toward the bulk equilibrium state. Surface segregation could be responsible for the absence of LRO and could cause Co clustering into platelets for all crystallographic orientations. In the absence of significant bulk atomic mobility, the surface arrangement would be ''frozen'' into the as-deposited sample. Previous workers, including ourselves, have suggested an interplay between surface diffusion and limited bulk atomic mobility as being the driving force in producing perpendicular anisotropy.[3,6,7,19]

We were not able to observe direct evidence of platelet formation with TEM. Thin platelets in principle might result in lateral strain variations or periodicities that might be detected in plan-view transmission images or diffraction patterns. However, if they are very thin and there are many overlapping platelets, they would be difficult to resolve.

Annealing experiments, shown in part in Fig. 12, demonstrate that at temperatures at or above 400 °C, anisotropy and clustering relax away into known bulk phases with no PMA. Annealing below 400 °C does not affect any of the samples (even those deposited at temperatures below the subsequent annealing temperature). 400 °C is approximately $T_m/3$, where T_m is the alloy melting temperature and, hence, is the expected temperature for the onset of significant bulk atomic mobility on laboratory time scales. For growth temperatures above 400 °C, we suggest that clustering may still occur at the surface during growth, but is annealed away during the deposition, resulting in the sharply dropping magnetic onset temperatures and the disappearance of PMA seen above 400 °C. Our annealing results show that anisotropy disappears much faster than clustering. Viewed in the context of the thin platelet model, this would imply that the Co/Pt interfaces are first disrupted before significant interdiffusion of Co and Pt occurs. It would make sense for the boundaries of the platelets to degrade before the entire platelet mixed into the alloy. Annealing at temperatures even slightly higher than 400 °C (450 °C for 100 h) drives samples grown at all temperatures toward bulk equilibrium. The sample with partial LRO in the as-deposited state changes the least, but all samples end up with a lower Curie temperature, indicating the presence of LRO in the annealed samples. The dramatic change seen in the film originally deposited at 200 °C and subsequently annealed is probably due to the larger number

of structural defects in that sample, which provide annealing channels along which atomic diffusion can proceed faster. It is clear that independent of the initial state of chemical order in the film (clustered, partial LRO, or fcc), annealing drives the alloy toward the accepted equilibrium state (LRO or fcc, depending on temperature) and destroys anisotropy.

Chemical LRO is found in as-deposited samples grown only at temperatures between 500 and 685 °C (the $L1_2$ chemical order-disorder transition).[26,27] The width of the $L1_2$ LRO peaks (from x-ray diffraction) is broad, implying small LRO domain sizes. The domain size calculated from these widths is consistent with the size expected[15] in an initially chemically disordered sample annealed at the growth temperature for the duration of the deposition (1.5 h). This observation suggests that $L1_2$ LRO *is formed only in the subsurface portion* of these samples due to annealing during deposition, due perhaps to surface segregation suppressing LRO at the growth surface.

The deposition rate experiments also suggest that surface atomic mobility determines the amount of anisotropy in as-deposited samples. At 250 °C, where significant PMA first appears in the as-deposited samples, slowing the deposition rate (thus allowing more time for each new monolayer to access the low-energy configuration) results in a significant PMA increase. A possible mechanism explaining this anisotropy increase could be the sharpening of the Co/Pt interfaces. At faster deposition rates the formation of clean Co/Pt interfaces could be kinetically limited, resulting in a loss of anisotropy in the overall sample. It is not clear why the increase of PMA at slower deposition rates is not accompanied by greater clustering, but it is possible that the amount of clustering is less sensitive to surface atomic mobility than is the quality of the interfaces. Varying the deposition rate at 400 °C produces no change in the magnetic properties of the sample, possibly because the surface reaches an equilibrium quickly at this temperature.

SUMMARY

We have deposited epitaxial (100), (110), (111), and polycrystalline $Co_{0.25}Pt_{0.75}$ and $Co_{0.35}Pt_{0.65}$ films on (100) and (110) MgO, (100) NaCl, (0001) Al_2O_3, and amorphous SiN, respectively, over a range of growth temperatures from −50 to 800 °C at deposition rates from 0.01 to 1.5 Å/s. Films grown at −50 and 80 °C and films grown at or above 700 °C are chemically disordered, homogeneous fcc phase. $L1_2$ long-range chemical order is present in as-deposited films grown at $550\,°C < T_S < 700\,°C$ and reaches its maximum value in those films grown at 630 °C ($S=0.65$); the LRO domain width is small, however. Films grown between 200 and 450 °C show dramatic growth-induced properties which vanish with annealing, including an enhanced Curie temperature (up to 400 °C onset) and low-temperature saturation magnetization (up to $2.7\mu_B$ per unit cell), perpendicular anisotropy (up to 7×10^6 ergs/cm^3), coercivity, and Kerr rotation. The magnetic properties indicate significant Co clustering, with a magnitude which is perfectly correlated with perpendicular anisotropy and anticorrelated with LRO. We find no qualitative difference in clustering or anisotropy in the three sample orientations: (100), (110), and (111).

We propose that the clustering takes the form of thin (two to three monolayers) flat platelets of fcc Co within a Pt-rich matrix, caused by aggregation of Co atoms at the growth surface, independent of crystallographic orientation. While there is no direct structural evidence for these platelets, the magnetic properties (enhanced saturation magnetization, Kerr rotation, Curie temperature, coercivity, and perpendicular anisotropy) are all explained by and consistent with this model. The platelets must be relatively small and incoherent with each other, resulting in x-ray and TEM measurements of a random fcc solid solution. Annealing and deposition rate experiments suggest that the sharpness of the interfaces, which determines the magnitude of the anisotropy, may be more easily destroyed than the platelets themselves. The formation of clustered Co networks on the surface during deposition may be related to the phenomenon of surface segregation. At deposition temperatures below the onset of significant bulk atomic mobility, the growth-surface-driven arrangement of Co clusters is ''frozen in'' by subsequent deposition. Annealing eliminates the platelets, driving the system toward either LRO or a chemically disordered fcc state depending on annealing temperature. Deposition rate experiments point to surface atomic mobility as the determining factor in the amount of anisotropy in as-deposited samples.

ACKNOWLEDGMENTS

We would like to thank R. F. C. Farrow and G. Harp for their helpful advice on Co_xPt_{1-x} epitaxy, G. Waychunas for useful discussions on x-ray scattering, V. Dharmavaram, B. B. Maranville, D. P. Arovas, A. Rosengren, A. Zangwill, N. Berker, and R. C. Dynes for valuable discussions, F. Deng and S. S. Lau for Rutherford backscattering analysis, V. Harris for EXAFS analysis, and E. Yu for atomic force microscopy. This work was supported by DOE Grant No. DE-FG03-95ER45529, the UC Campus–Laboratory Collaboration Program, and the NSF-MRL program through the Center for Materials Research at Stanford University, and benefited from the use of facilities provided by the Center for Magnetic Recording Research at U.C. San Diego and by the Center for Materials Research at Stanford University.

[1] C. J. Lin and G. Gorman, Appl. Phys. Lett. **61**, 1600 (1992).

[2] D. Weller, H. Brandle, G. Gorman, C-J Lin, and H. Notarys, Appl. Phys. Lett. **61**, 2726 (1992).

[3] D. Weller, H. Brandle, and C. Chappert, J. Magn. Magn. Mater. **121**, 461 (1993).

[4] E. E. Marinero, R. F. C. Farrow, G. R. Harp, R. H. Geiss, J. A. Bain, and B. Clemens, in *Magnetic Ultrathin Films: Multilayers and Surfaces/Interfaces and Characterization*, edited by B. T. Jonhen *et al.*, MRS Symposia Proceedings No. 313 (Materials Research Society, Pittsburgh, 1993), p. 677.

[5] R. F. C. Farrow, D. Weller, M. F. Toney, T. A. Rabedeau, J. E. Hurst, G. R. Harp, R. F. Marks, R. H. Geiss, and H. Notarys, in

Polycrystalline Thin Films: Structure, Texture, Properties and Applications, edited by K. Laemak *et al.*, MRS Symposia Proceedings No. 343 (Materials Research Society, Pittsburgh, 1994), p. 375.

[6] P. W. Rooney, A. L. Shapiro, M. Q. Tran, and F. Hellman, Phys. Rev. Lett. **75**, 1843 (1995).

[7] M. Maret, M. C. Cadeville, R. Poinsot, A. Herr, E. Beaurepaire, and C. Monier, J. Magn. Magn. Mater. **166**, 45 (1997).

[8] Li Ming, Jiang Zhihong, Zou Zhiqiang, and Shen Defang, J. Magn. Magn. Mater. **176**, 331 (1997).

[9] Y. Yamada, T. Suzuki, and E. N. Abarra, IEEE Trans. Magn. **MAG-33**, 3622 (1997).

[10] R. F. C. Farrow, R. F. Marks, A. Cebollada, G. R. Harp, T. A. Rabedeau, M. F. Toney, D. Weller, and S. S. P. Parkin, J. Cryst. Growth **150**, 1126 (1995).

[11] F. Hellman, A. L. Shapiro, E. N. Abarra, P. W. Rooney, and M. Q. Tran, in MORIS Conference Proceedings [J. Magn. Soc. Jpn. **23** Suppl. S1, 79 (1999)].

[12] S. Hashimoto, Y. Ochiai, and K. Aso, J. Appl. Phys. **67**, 2136 (1990).

[13] W. B. Zeper, F. J. A. M. Grenadius, P. F. Garcia, and C. R. Fincher, J. Appl. Phys. **65**, 4971 (1989).

[14] M. Hansen and K. Anderko, *Constitution of Binary Alloys* (McGraw-Hill, New York, 1958), pp. 467 and 516.

[15] H. Berg and J. B. Cohen, Metall. Trans. **3**, 1797 (1972).

[16] G. R. Harp, D. Weller, T. A. Rabedeau, R. F. C. Farrow, and M. F. Toney, Phys. Rev. Lett. **71**, 2493 (1993).

[17] A. L. Shapiro, B. B. Maranville, V. Dharmavaram, and F. Hellman (unpublished).

[18] T. A. Tyson, S. D. Conradson, R. F. C. Farrow, and B. A. Jones, Phys. Rev. B **54**, 3702 (1996).

[19] C. Meneghini, M. Maret, M. C. Cadeville, and J. L. Hazemann, J. Phys. IV **7**, C2-1115 (1997); C. Meneghini, M. Maret, V. Parasote, M. C. Cadeville, J. L. Hazemann, R. Cortes, and S. Colonna, Eur. Phys. J. B **7**, 347 (1999).

[20] W. Grange, M. Maret, J.-P. Kappler, J. Vogel, A. Fontaine, F. Petroff, G. Krill, A. Rogaler, J. Goulon, M. Finazzi, and N. B. Brookes, Phys. Rev. B **58**, 6298 (1998).

[21] U. Bardi, A. Atrei, E. Zanazzi, G. Rovida, and P. N. Ross, Vacuum **41**, 437 (1990); U. Bardi, B. C. Beard, and P. N. Ross, J. Catal. **124**, 22 (1990).

[22] M. Galeotti, A Atrei, U. Bardi, B. Cortigiani, G. Rovida, and M. Torrini, Surf. Sci. **297**, 202 (1993).

[23] The substrate temperature of the low-temperature film was −85 °C at the beginning of the deposition and rose to −40 °C by the end of the deposition (100 min elapsed time). We have chosen to define the substrate temperature of this film as −50 °C. All of the other films were held within 4 °C of the reported substrate temperature throughout the deposition. The temperature was monitored with two *K*-type thermocouples mounted directly on the sample plate.

[24] V. G. Harris, K. M. Kemner, A. L. Shapiro, and F. Hellman (unpublished).

[25] M. C. Cadeville, C. E. Dahmani, and F. Kern, J. Magn. Magn. Mater. **54-57**, 1055 (1986).

[26] J. M. Sanchez, J. L. Moran-Lopez, C. Leroux, and M. C. Cadeville, J. Phys.: Condens. Matter **1**, 491 (1989).

[27] J. Crangle and W. R. Scott, J. Appl. Phys. **36**, 921 (1965).

[28] F. Menzinger and A. Paoletti, Phys. Rev. **143**, 365 (1966).

[29] D. Weller, Y. Wu, J. Stohr, M. G. Samant, B. D. Hermsmeier, and C. Chappert, Phys. Rev. B **49**, 12 888 (1994).

[30] H. Miyajima, K. Sato, and T. Mizoguchi, J. Appl. Phys. **47**, 4669 (1976).

[31] H. Braendle, D. Weller, S. S. P. Parkin, J. C. Scott, P. Fumagalli, W. Reim, R. J. Gambino, R. Ruf, and G. Güntherodt, Phys. Rev. B **46**, 13 889 (1992).

[32] C. Kooy and U. Enz, Philips Res. Rep. **15**, 7 (1960).

[33] V. Gehanno, Y. Samson, A. Marty, B. Gilles, and A. Chamberod, J. Magn. Magn. Mater. **172**, 26 (1997).

[34] J. U. Thiele, L. Folks, M. F. Toney, and D. K. Weller, in *High-Density Magnetic Recording and Integrated Magneto-Optics: Materials and Devices*, edited by K. Rubin *et al.*, MRS Symposia Proceedings No. 517 (Materials Research Society, Pittsburgh, 1998), p. 319.

[35] C. M. Schneider, P. Bressler, P. Schuster, J. Kirschner, J. J. de Miguel, and R. Miranda, Phys. Rev. Lett. **64**, 1059 (1990).